30, 551 (1966).
9. L. Pauling, *J. Phys. Chem.*, **56**, 361 (1962).
10. D. O. Raleigh, *This Journal*, **113**, 782 (1966).
11. T. Mills and F. A. Kroger, *ibid.*, **120**, 1582 (1973).
12. W. C. Tripp *et al.*, Final Report ARL TR75-0130 June 1975.
13. C. Wagner, in "Proceedings of the 7th Meeting of the International Committee on Electrochemistry, Thermodynamics, and Kinetics," Lindau 1955.
14. J. B. Wagner, Jr. and C. Wagner, *J. Chem. Phys.*, **26**, 1597 (1957).
15. H. F. Wolf, "Silicon Data Handbook," Pergamon Press, New York (1969).
16. J. T. Law, *J. Phys. Chem.*, **61**, 1200 (1957).
17. F. M. Folkes, Abstract 166, p. 437, The Electrochemical Society Extended Abstracts, Vol. 80-1, St. Louis, MO, May 6-11, 1980.
18. R. Pfeffer and M. Ohring, *J. Appl. Phys.*, **52**, 777 (1981).
19. S. K. Ghandhi, "The Theory and Practice of Microelectronics," p. 140, John Wiley and Sons, New York (1968).
20. D. R. Lamb, *Thin Solid Films*, **5**, 247 (1970).
21. B. E. Deal and A. S. Grove, *J. Appl. Phys.*, **36**, 3770, 1965.

Some Applications of Cold Crucible Technology for Silicon Photovoltaic Material Preparation

T. F. Ciszek*

Solar Energy Research Institute, Golden, Colorado 80401

ABSTRACT

Cold crucible melt confinement was used for four different silicon crystallization methods of interest in photovoltaic material preparation: directional solidification, Czochralski pulling, sheet growth, and continuous ingot casting. Large grained, multicrystalline ingots were directionally solidified in cold crucibles, and grain sizes up to 5 mm were observed. Dislocation-free crystals were pulled in [111] and [100] orientations, using semiconductor-grade silicon. The edge-supported pulling (ESP) growth method was employed for sheet growth. The sheets were solidified between quartz filaments. Continuous casting of square cross-sectional ingots with grain sizes of up to several millimeters was carried out. Material suitable for fabrication into solar cells was obtained by these methods. AM1 solar cell IV characteristics are presented for the different materials and for coprocessed cells made from conventional Czochralski crystals grown using quartz crucibles. Some purity and electrical property data for cold crucible crystals are also given. Dislocation-free cold crucible crystals had higher purity levels and photovoltaic conversion efficiencies than conventional Czochralski crystals.

The importance of high efficiency to viable photovoltaic systems is becoming progressively more recognized. With silicon, several researchers have already realized AM1 efficiencies above 18%. Because of its abundance, low material cost, salubrity, established technology base, and high theoretical conversion efficiency, silicon is an excellent candidate material for high efficiency PV systems. However, the minority carrier lifetime attainable in heavily doped (<0.5 Ω-cm) Czochralski-grown crystals from quartz crucibles may not be adequate for high efficiency solar cells. This paper explores some roles that cold crucible technology might play in silicon material preparation for both dislocation-free single-crystal cells and multicrystalline cells (including silicon sheets). Cold crucible growth shows a potential for less impurity incorporation than Czochralski growth because, in the former method, there are no hot reactive surfaces near the molten silicon. In addition, radio frequency (RF) repulsion tends to push the liquid silicon away from the finger-like water-cooled walls of the melt container.

Cold crucible melt confinement was used for four different silicon crystallization methods of interest in photovoltaic material preparation: directional solidification, Czochralski pulling, sheet growth, and continuous casting. Solar cells were fabricated from the crystallized silicon and compared with solar cells fabricated on conventional Czochralski-grown (CZ) wafers.

Experimental

Principles of cold crucible operation.—Heating and melt confinement with cold crucibles is provided via RF induction heating. In this study, a 65 mm diam RF coil with five turns was used at 470 kHz. The coil surrounds the cold crucible coaxially. The vertical walls of the crucible are composed of closely spaced, electrically isolated, water-cooled copper fingers that have approximately square cross sections. Each finger acts as an RF stepdown transformer, and the coil current induces RF currents to flow in the fingers. The finger currents, in turn, induce a current to flow in the silicon charge. Heating and melting of the charge is caused by ohmic resistance to this current flow (I^2R heating). At the inside wall of the crucible, the instantaneous current directions in the fingers and in the charge are opposed (Fig. 1). Thus, a force arises due to magnetic repulsion and the silicon melt is pushed away from the fingers.

Directional solidification.—For directional solidification or Stockbarger-type growth of large grained, multicrystalline silicon, a commercial cold crucible with a 31 mm id, a 50 mm od, and a hemispherical bottom was used. The cross section of each water-cooled finger is a sector of a right cylindrical annulus, as shown in Fig. 1. The inner radii of the sectors decrease in the hemispherical bottom region until the cross section becomes a wedge at the very bottom. The crucible is made of copper with gold plating. A flared, cylindrical, fused-quartz sheath was placed between the cold crucible and the RF coil, with the flared portion extending outward over the top of the coil, to prevent arcing between the coil and crucible. The assembly was housed in a 38 cm diam, water-cooled, stainless-steel growth chamber. The crucible and coil were stationary.

A 55g charge of semiconductor-grade silicon along with sufficient boron dopant to yield approximately 2 Ω-cm resistivity was placed in the crucible. The growth chamber was evacuated before it was filled with 99.999% minimum-purity argon at 1.2 bar total pressure. The silicon charge was preheated with a graphite heater, inductively coupled to the top of the cold crucible, until it was hot enough to couple directly to the cold crucible. At this point, the preheater was moved away from the crucible region.

An RF power level of 19.5 kW (6.1 kV plate voltage and 3.2A plate current) was used to melt and stabilize the polycrystalline silicon. For directional solidification, the power was ramped down to 0 at a rate of approximately 0.5 kW/min. Figure 2 shows an etched cross section of an

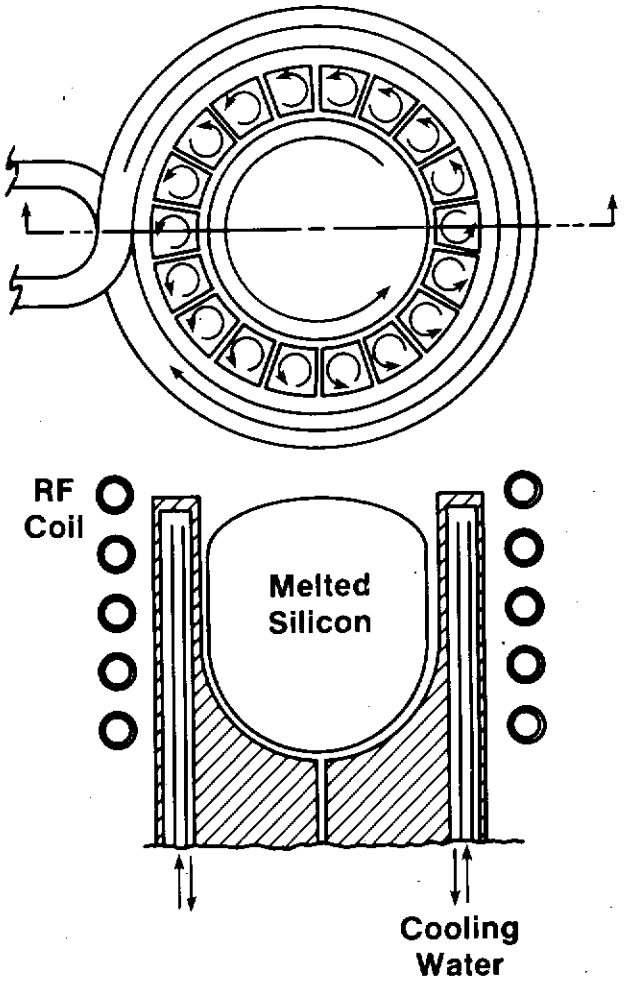

Fig. 1. Operating principle of a cold crucible showing instantaneous current flows.

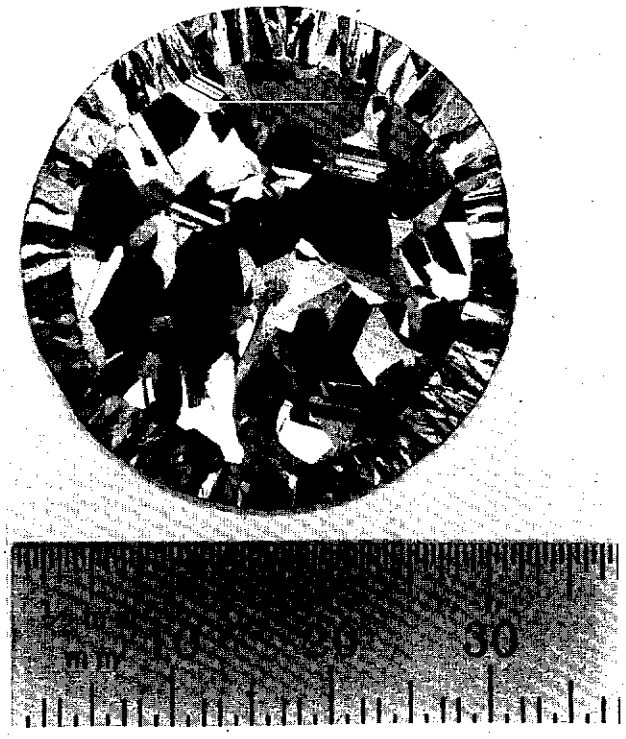

Fig. 2. Etched cross section of silicon directionally solidified in a cold crucible.

ingot solidified in this manner. Grain sizes of up to 5 mm can be seen.

Czochralski pulling.—While silicon crystals had previously been CZ pulled from a cold crucible (1), auxiliary radiant heating with a graphite heater was required for seeding. Auxiliary heating may compromise the purity of the grown crystals by increasing the carbon content, for example. In this study, both [100] and [111] dislocation-free crystals were grown without auxiliary heating from a cold crucible system similar to the one used for directional solidification of silicon.

Seeds with 4 × 4 mm square cross sections and either [111] or [100] orientation were used. At a generator power level of 20.5 kW (plate voltage = 6.2 kV, and plate current = 3.3A), a 60g charge of melted silicon in the cold crucible was sufficiently hot to allow good wetting on the rotating seed. When even wetting was achieved, the seed was pulled upward initially at 3 mm/min. Then the power was dropped to 19.2 kW, and the pulling speed was increased to approximately 20 mm/min in order to grow a thin-necked crystal of 1.3-2.5 mm diam and more than 2 cm long. Necks grown under these conditions were sufficient to eliminate dislocations generated in the seed attachment region and allowed subsequent growth to be dislocation-free. A rotation rate of 13 rpm was used.

After the neck was grown, the pulling speed and power were adjusted to widen the crystal to about 15 mm diam, and the rotation rate was reduced to around 5 rpm. Figure 3 shows the hot zone during the diameter transition. In addition to pushing the melt away from the cold crucible fingers, magnetic repulsion also causes the top of the melt to be nearly hemispherically domed in such a small crucible; therefore, growing crystals with diameters larger than about 15 mm is difficult. At full diameter, growth speeds from 0.2-2.8 mm/min were tried, and the power levels used ranged from 11 to 14 kW. Some crystals were doped with boron to approximately 2 Ω-cm resistivity, for solar cell use.

Silicon sheet growth.—The edge-supported pulling (ESP) growth method (2-4) was employed for sheet growth, and, again, the crucible configuration was similar to that described for directional solidification. The silicon sheets were solidified between 0.5 mm diam quartz capillary filaments that had 0.02 mm wall thicknesses. The filaments were spaced 17 mm apart. Growth was initiated on a single-crystal seed sheet mounted between the filaments, and then the seed/filament assembly was moved upward at 15-30 mm/min to grow the sheet.

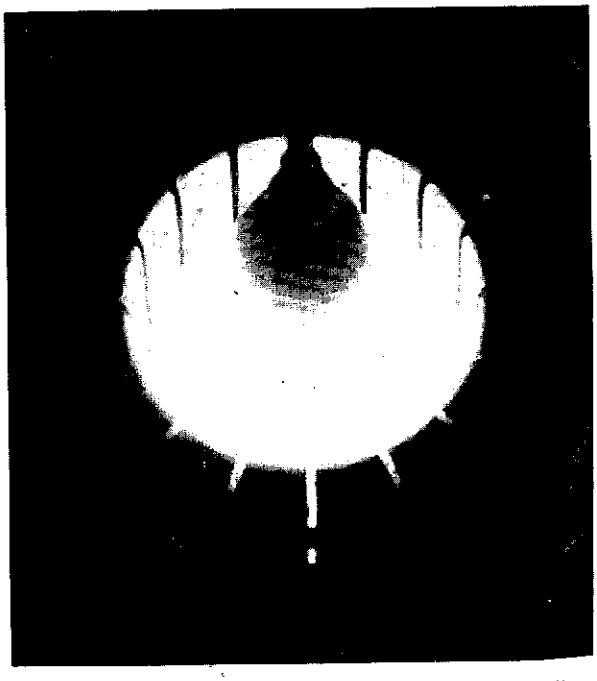

Fig. 3. Cold-crucible Czochralski pulling of dislocation-free silicon

A very high meniscus was observed, because the magnetic repulsion tends to create a mounded upper melt surface and also because there is a melt rise to the sheet's solid/liquid interface of 6-7 mm in addition to the RF effect. Under these harsh thermal gradients, the sheet quickly became multicrystalline. A larger crucible would be advantageous. Because the thin-walled quartz filaments are relatively weak, thermal expansion mismatch between them and the silicon sheet causes the filaments to break away from the sheet during cooldown and a straight sheet edge is left (Fig. 4).

Continuous casting.—The three crystallization methods described so far used a round cold crucible with a closed bottom. Continuous casting of silicon ingots was performed in an open-bottom crucible having a 26 × 26 mm square confinement cross section with slightly octahedral corners. The vertical water-cooled copper fingers were 6 × 6 mm in cross section and 104 mm high. A five-turn RF coil was used that had two outer turns with an 83 mm id and three inner turns with a 61 mm id. The coil was 38 mm high and was placed with its midplane 34 mm below the tops of the fingers. A cylindrical quartz arc shield was concentrically located between the cold crucible and the RF coil.

The casting process was started by inserting a 25 × 25 mm square graphite support into the bottom of the open crucible until it was at midcrucible height. 12g of silicon were placed on the support. The growth chamber was evacuated and purged with argon. Then the RF coil was energized to heat the graphite, which in turn heated the silicon, until the silicon was hot enough to couple directly to the cold crucible. An RF power level of 10.3 kW (at 464 kHz) was adequate to melt the silicon. At that point, the addition of new silicon material through the open top of the crucible was begun at a rate of 240 g/h, the RF power level was increased to 15.7 kW, and the graphite support was started downward at 2.5 mm/min. The liquid silicon solidified as it was slowly lowered out of the RF field, at a rate equal to the raw silicon addition rate. The process was operated for over an hour. Figure 5 is a schematic of the continuous casting process. Figure 6 shows a cast silicon ingot that is 17 cm long and has a square cross section. Grain sizes of up to several millimeters were observed.

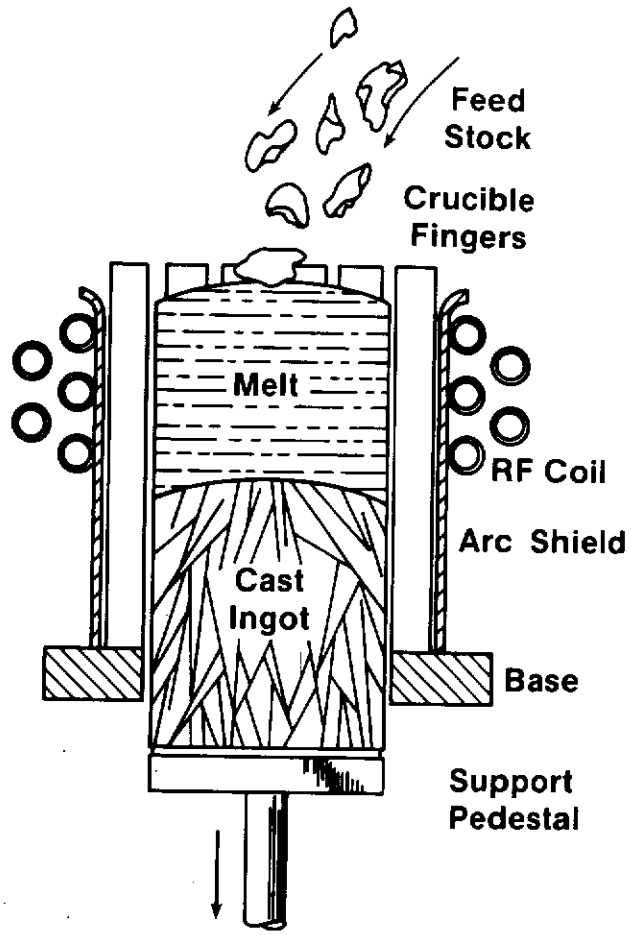

Fig. 5. Schematic diagram of a cold-crucible continuous casting process.

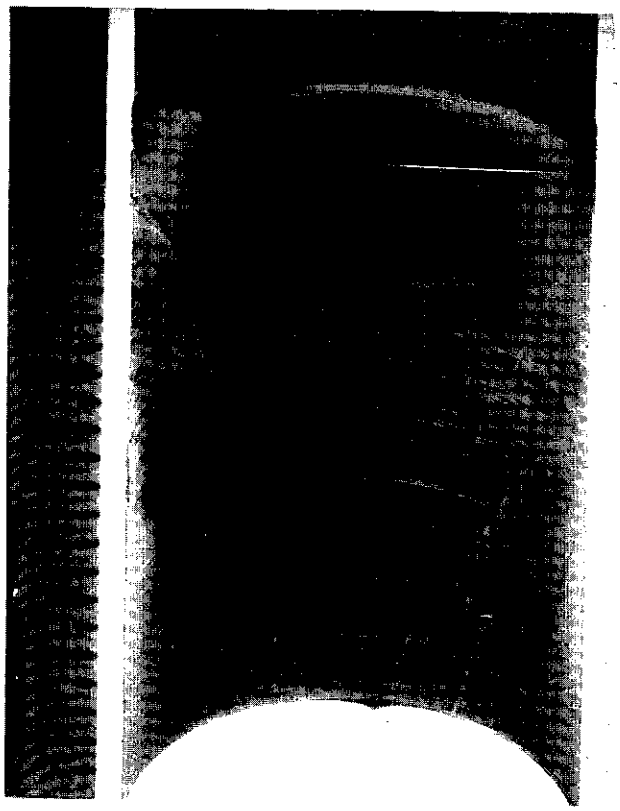

Fig. 4. An ESP silicon sheet grown from a cold crucible using quartz filaments.

Results

Properties measurements.—A number of characterization techniques were used to evaluate the CZ-pulled crystals. X-ray topograpy was used to examine the defect structure of the crystals. Molybdenum-K_{α_1} radiation from a line-focus tube operating at 40 kV and 30 mA was

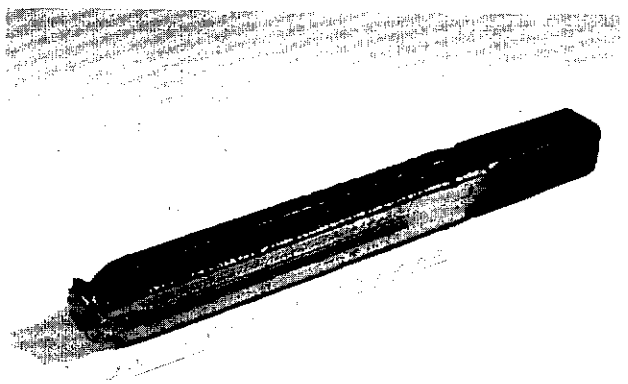

Fig. 6. A continuously cast cold crucible ingot, 17 cm long by 2.5 cm square.

used to image (220) scanning transmission topographs on Ilford L-4 photographic plates. It was verified that the neck growth procedure described in the Czochralski pulling section was sufficient to establish dislocation-free growth in both [111] and [100] orientations, and that the crystals remained dislocation-free at full diameter.

The feed-stock silicon for the cold crucible was semiconductor-grade material. An undoped [111] dislocation-free crystal was determined to be p-type with 90-200 Ω-cm resistivity, indicating an excess acceptor impurity content of approximately 1×10^{14} atom/cm³. The minority carrier bulk lifetime of this crystal, as measured by the ASTM photoconductive attenuation method, was 195 μs. Some crystals were doped with boron, during growth, to between 2 and 3 Ω-cm p-type for solar cell evaluation. Infrared transmission spectroscopy analysis for carbon and oxygen impurities showed none above the levels in a vacuum float-zoned reference wafer. Neutron activation analysis for gold and copper in a [100], 2.5 Ω-cm, dislocation-free single crystal grown from the gold-plated copper cold crucible indicated a level of 0.14 ppb (weight) for gold and 15.0 ppb (weight) for copper.

Room temperature Hall mobility measurements were made on a polished wafer from one of the [100], dislocation-free, boron-doped crystals. Indium/tin alloy contacts were used with van der Pauw's method for disks of arbitrary shape (5). The measurements indicated a p-type carrier concentration of 8.3×10^{15}/cm³ and a resistivity of 2.55 Ω-cm. From three separate determinations, the average mobility was 295 cm²/V-s with a standard deviation of 4 cm²/V-s.

Solar cell characteristics.—Material suitable for fabrication into solar cells was obtained by three of the cold crucible methods. The continuously cast material was not doped, and no cells were fabricated. However, when properly doped, these ingots are expected to be similar in cell performance to the directionally solidified silicon.

Cold-crucible-grown silicon wafers were cut, lapped, machine polished with a colloidal silica slurry, and used to fabricate solar cells. Control cells, using commercial CZ-grown wafers of similar resistivity, were processed along with the cold-crucible-grown silicon. The cell fabrication process consisted of a phosphorus oxychloride diffusion at 850°C that created a 0.3 μm deep junction with approximately 90 Ω/□ sheet resistance, an aluminum drive-in back contact, and photolithographically defined front metallization. A standard Ti/Pd/Ag evaporated grid deposition sequence was used for the front contact. The cell areas ranged from 0.1 to 3.0 cm². The smaller cells were mesa array cells fabricated simultaneously on a wafer. Individual cells in an array were isolated by an etched moat. Figure 7 shows the completed device array configuration. To better determine material effects on cell efficiency, antireflection (AR) coatings were generally not used.

Directionally solidified material ("Directional solidification" section, above) was large grained (see Fig. 2). Mesa-defined cells 1.61 cm² in area were cofabricated on both round directionally solidified wafers and commercial CZ controls of similar resistivity. Typical uncoated I/V characteristics under ELH lamp illumination at an intensity of 100 mW/cm² and a temperature of 25°C are shown in Fig. 8. Poorer performance in short-circuit current density (J_{sc}), open-circuit voltage (V_{oc}), and fill factor (FF) result in an efficiency of only 9.2% for the directionally solidified cell *vs.* 10.8% for the CZ control. AR coatings are expected to increase these values to approximately 13% and 15.4%, respectively.

Solar cell efficiencies for cold-crucible-pulled CZ crystals were observed to be higher than those of coprocessed, conventional CZ crystals. The characteristics of 0.1 cm² mesa array cells were again measured without an AR coating, so that any differences due to substrate material would not be masked by potential AR coating variations. Statistics on cell performance at 25°C under tungsten ELH lamp illumination, and at 28°C under filtered xenon solar simulator illumination, both at 100 mW/cm² intensity, are given in Table I. Cell results from several wafers are included. In all cases, V_{oc}, J_{sc}, and cell efficiency were higher for the cold-crucible-grown material. The fill factors were nearly equal within the standard deviation (shown in parentheses) of the measurements. Under ELH illumination at 25°C, the average control efficiency was 10.9%; the cold crucible cells were 11.7% efficient. Under xenon solar simulator illumination at 28°C, the control cells were 10.2% efficient, and the cold-crucible cells had an average efficiency of 10.6%. Good AR coatings can increase the cell efficiency values by at least 43% and as much as 50% (6) if combined with surface passivation. Two larger cells were made from a CZ control wafer and a cold-crucible CZ wafer (3.04 and 0.64 cm² respective cell areas). These cells were fabricated using a relatively low efficiency base-line process, and a simple one-layer AR coating was applied. The comparative performance under 100 mW/cm² ELH illumination at 25°C is shown in Fig. 9 and indicates an 8% advantage for the cold-crucible cell under these processing and measurement conditions.

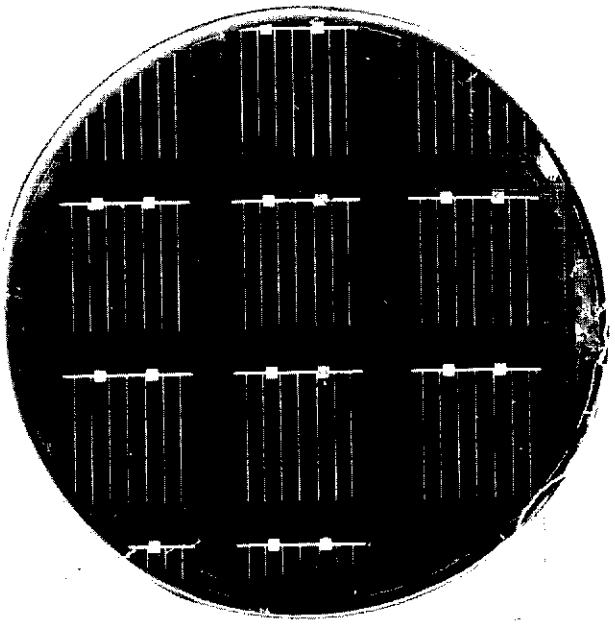

Fig. 7. An array of 0.10 cm² mesa cells on a [100] cold crucible Si wafer.

In Fig. 10, a comparison is made between several conventional CZ control cells and cold-crucible ESP sheet cells. Again, the cells are not AR-coated. In this case, a 0.1 cm² mesa array cell structure is used. The range of performance for the ESP cells correlates with the crystal structure (nearly single-crystal regions exhibit the best performance—up to 90% of the control efficiencies—while the smaller grained regions near the filaments have the lowest solar cell efficiency—as little as 68% of the control efficiencies).

Summary and Discussion

The cold-crucible method with RF heating has been successfully applied to the crystallization of silicon in

Table I. Solar cell current/voltage characteristics for some diffused-junction n/p devices of 0.10 cm² total area.

Cell Measurement Conditions	Cell Description	No. of Cells	V_{oc} (mV)	J_{sc} (mA/cm²)	FF (%)	Eff. (%)
100 mW/cm², ELH lamps, 25°C, no AR coating, 0.1 cm² cell area	Cz Control	3	573(±1)	23.8(±.2)	80(±1)	10.9(±.3)
	Cold Crucible	8	579(±3)	24.9(±.4)	81(±1)	11.7(±.2)
100 mW/cm² SERI filtered Xenon simulator 28°C, no AR coating, 0.1-cm² cell area	Cz Control	3	561(±.4)	22.9(±.1)	79.4(±.3)	10.2(±.1)
	Cold Crucible	4	568(±.7)	23.5(±.4)	78.9(±.2)	10.6(±.2)

Fig. 8
cell.

four
mm
materi
about
cells.
pulled
crucibl
to gro
dislocat
the cry
propert
made
may ha
pendin
conven
taic ap
pulled
and qu
were
those
The eff
larger
A ne
bottom

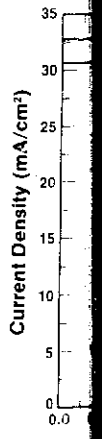

Fig. 9
CZ cells.

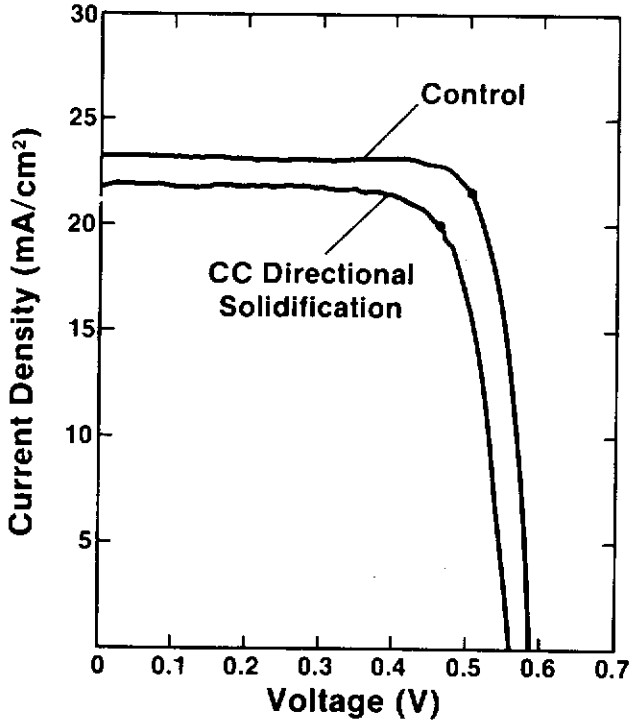

Fig. 8. I/V curves for a CZ control cell and a directionally solidified cell.

four different ways. Directional solidification yielded 30 mm diam, 55g ingots with grain sizes of up to 5 mm. This material was made into solar cells having efficiencies about 85% as good as those of conventional CZ control cells. Dislocation-free, 15 mm diam silicon crystals were pulled in both [111] and [100] orientations by a cold-crucible CZ technique. No auxiliary heating was required to grow the thin necks that are necessary to initiate dislocation-free crystals. X-ray topography verified that the crystals were dislocation-free. A number of electrical property measurements, and an analysis of solar cells made from the crystals, indicate that cold-crucible silicon may have some device efficiency advantages (4%-8%, depending on processing and illumination conditions) over conventional Czochralski-grown substrates for photovoltaic applications. Silicon sheets 17 mm wide were also pulled from a cold crucible melt using the ESP technique and quartz filaments. Pulling speeds of 15-30 mm/min were used. Solar cell efficiencies 68%-90% as good as those of conventional CZ control cells were observed. The efficiency was a function of sheet grain size, with larger grained areas having higher efficiencies.

A new continuous casting method using an open-bottom cold crucible was applied to silicon. Ingots 25 × 25 mm in cross section and 17 cm long were cast at a linear rate of 2.5 mm/min and had grain sizes of up to several millimeters. This technique should be applicable to many other materials that are electrically conductive in the molten state. A variety of feedstock geometries such as liquid melts, solid bars, pellets, and powders could be used. The solid/liquid interface is submerged and hence slag formation that occurs in some solidification processes could be kept away from the interface. Contamination levels would also be lower than those in conventional casting processes. Long ingots with tailored cross-sectional shapes can be produced.

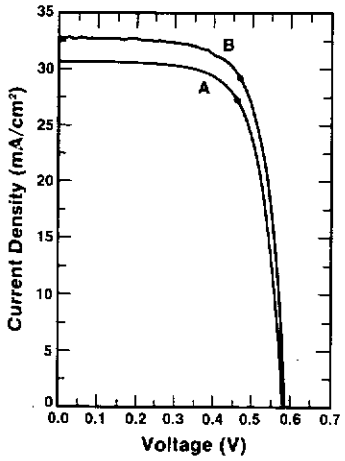

	CZ Control Cell A	Cold Crucible Cell B
V_{oc}	0.577 V	0.583 V
I_{sc}	93.1 mA	20.9 mA
J_{sc}	30.6 mA/cm²	32.9 mA/cm²
V_{mp}	0.462 V	0.467 V
I_{mp}	83.0 mA	18.6 mA
P_{max}	38.3 mW	8.7 mW
FF	0.71	0.71
Eff	12.6%	13.7%

Fig. 9. I/V curves for coprocessed conventional CZ and cold crucible CZ cells.

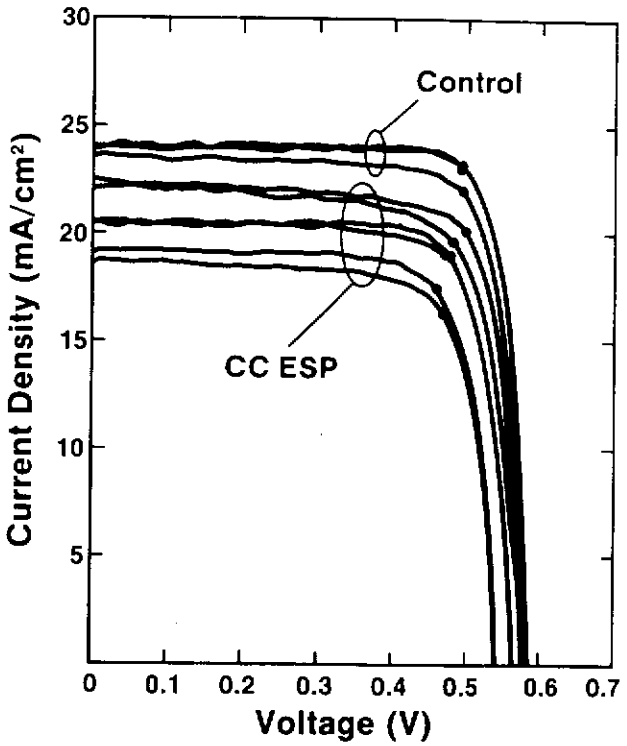

Fig. 10. I/V curves for six ESP cold crucible cells and three CZ control cells.

The main advantage that cold-crucible silicon melt confinement holds over conventional crucible techniques is freedom from high levels of impurities such as oxygen and carbon. Crystal purities appear to approach those of float-zoned crystals for C and O. Neutron activation analysis indicated that no significant contamination was introduced in the silicon crystals from the copper or gold cold-crucible material.

All of the work reported here was done with relatively small cold crucibles (approximately 30 mm diam). Considerable scale-up would be necessary for commercial application. This should not be a major problem, since cold crucibles up to 45 cm diam have been used in skull melting applications.

Acknowledgments

The assistance of the following three individuals is especially appreciated: M. Schietzelt, who provided help with the crystallization experiments; J. L. Hurd, who performed the infrared analysis and helped with design detailing and fabrication of the open-bottom cold crucible; T. Schuyler, who did the solar cell fabrication and testing. In addition, the author thanks C. Osterwald for carrying out the SERI solar simulator cell measurements. Support for this work was provided by the U.S. Department of Energy under Contract DE-AC02-83CH10093 and, in part, by JPL Contract WO8746-83.

Manuscript received Oct. 1, 1984. This was Paper 336 presented at the New Orleans, Louisiana, Meeting of the Society, Oct. 7-12, 1984.

Solar Energy Research Institute assisted in meeting the publication costs of this article.

REFERENCES

1. J. F. Wenckus and W. P. Menashi, Final Technical Report RADC-TR-82-171, Rome Air Development Center, Hanscom AFB, MA (1982).
2. T. F. Ciszek and J. L. Hurd, in "Electronic and Optical Properties of Polycrystalline or Impure Semiconductors and Novel Silicon Growth Methods," K. V. Ravi and B. O'Mara, Editors, p. 213, The Electrochemical Society Softbound Proceedings Series, Pennington, NJ (1980).
3. T. F. Ciszek, J. L. Hurd, and M. Schietzelt, *This Journal*, 129, 2838 (1982).
4. J. L. Hurd and T. F. Ciszek, *J. Cryst. Growth*, 59, 499 (1982).
5. L. J. van der Pauw, *Philips Res. Rpts.*, 13, 1 (1958).
6. A. Rohatgi and P. Rai-Choudhury, Annual Report, SERI Contract XB-3-02090-4, Solar Energy Research Institute, Golden, CO (1984).

A Study of UV Absorption Spectra and Photolysis of Some Group II and Group VI Alkyls

S. J. C. Irvine, J. B. Mullin, D. J. Robbins,* and J. L. Glasper

Royal Signals and Radar Establishment, Great Malvern, Worcester, England WR14 3PS)

ABSTRACT

A preliminary study has been made of the UV photolysis of metal-organic compounds of Hg, Cd, and Te which could be used for low temperature, selective area deposition of cadmium mercury telluride (CMT). High resolution UV absorption spectra have been measured for dimethylcadmium ($CdMe_2$), dimethylmercury ($HgMe_2$), and diethyltelluride ($TeEt_2$). Possible modes for photodissociation are discussed in light of these results. The photodissociation of these alkyls was attempted in a hydrogen stream at atmospheric pressure using a mercury-xenon lamp, deposition being onto a silica reaction tube. Yields of Cd, Hg, and Te were measured under different deposition conditions to determine the dependence on UV intensity, alkyl concentration, and flow velocity.

Recent interest in low temperature growth of the infrared detector material cadmium mercury telluride (CMT) has stimulated research into new epitaxial growth techniques (1-3). The preliminary study of UV photolysis reported here is part of an investigation to use alkyls for the growth of CMT at temperatures where they are thermally stable (4, 5) and possibly achieve selective area growth.

The alkyl sources used for metal-organic vapor phase epitaxy (MOVPE) are dimethylcadmium ($CdMe_2$) and diethyltelluride ($TeEt_2$) with Hg vapor introduced from a liquid Hg source. Pyrolysis of these alkyls enables high growth rates of CMT at substrate temperatures above 400°C. In the present study, the UV absorption spectra of $CdMe_2$, $HgMe_2$, and $TeEt_2$ have been measured. Also, photolysis experiments have been attempted at room temperature using $CdMe_2$, $HgMe_2$, $HgEt_2$, $TeMe_2$, and $TeEt_2$.

Room temperature photodeposition of Cd from $CdMe_2$ was achieved by Jonah *et al.* (6) using a 1 kW xenon-mercury lamp, and in more recent studies Ehrlich *et al.* (7) used $CdMe_2$ for localized deposition of Cd using a CW laser source at 257 nm. The latter authors have also measured the UV absorption spectra of $CdMe_2$ in the vapor phase and as an adsorbed layer (8, 9). Multiphoton absorption of $CdMe_2$ has been claimed by Rytz-Froidevaux *et al.* (10), who used longer wavelength radiation (above 300 nm) to initiate Cd deposition onto a quartz window; the deposition proceeds by heat generated in the photodeposited film. This technique involves a surface selective reaction and can produce Cd deposition to a resolution better than 1 μm.

Experimental

In order to investigate the UV absorption processes leading to photodissociation, the absorption spectra of the alkyls $CdMe_2$, $HgMe_2$, and $TeEt_2$ were measured at room temperature in a stainless steel gas cell. This cell had a path length of 5.1 cm and was fitted with UV transmitting Spectrosil A quartz windows. The absorption cross section at a particular wavelength can be estimated from the absorption coefficient using the relation

$$\alpha_\lambda = N\sigma_\lambda$$

For an ideal gas at STP, $N = 2.77 \times 10^{19}$ molecules cm^{-3}

$$\therefore \sigma_\lambda \sim (0.27 \times 10^{-16}) \frac{\alpha_\lambda}{p} \text{ cm}^2$$

where p is the partial pressure of the alkyl measured in torr. In all the spectra given below, the broken line represents the absorption due to H_2 carrier gas only in the cell, and the solid line represents that of carrier gas with a small pressure p of the appropriate alkyl. The absorption coefficient α (cm^{-1}) for each alkyl is then given by the difference between these curves.

The spectral region of greatest interest is 200-300 nm. At longer wavelengths, the alkyls show negligible absorption, while at shorter wavelengths the Hg lamp used for dissociation emits negligible power. Absorption data in this spectral range have previously been obtained by Thompson and Linnett (11) using photographic techniques, but these spectra do not give the necessary information on relative strengths of transitions.

The photodeposition measurements were made using a continuous stream of H_2 plus alkyl vapor at a controlled flow rate and concentration and a constant total pressure of 1 atm. High purity hydrogen is supplied via flowmeters to two lines; one is fed to the bubbler containing the alkyl, the other line acts as a dilution stream to alter the partial pressure of alkyl vapor. The mixed stream is passed at ambient temperature through a 7 mm id silica tube. Radiation from a 1 kW Oriel mercury-xenon lamp was focused onto the silica tube. Waste gases from the reaction zone, predominantly hydrogen, are passed to a combustion chamber and burnt in a continuous flame. The whole system can be pumped out to test for leaks and purged with hydrogen. There were a number of additional features which were used in some of the experiments, such as back-reflecting mirror, masking, and a power meter. A laser power meter was used, with black body absorption characteristics to measure the radiation power density passing through the silica reaction tube.

The amounts of material deposited onto the wall of the silica tube as a consequence of photolysis were dissolved in acid and determined by atomic absorption analysis. The deposits were metallic in appearance and were not expected to contain large amounts of organic impurities, as subsequent secondary ion mass spectrometer (SIMS) experiments on epitaxial thin films only show small amounts of carbon contamination (18).

*Electrochemical Society Active Member.